Catalysis Today 350 (2020) 19–24

Contents lists available at ScienceDirect

Catalysis Today

journal homepage: www.elsevier.com/locate/cattod

Understanding the conversion of ethanol to propene on In_2O_3 from first principles

Runhong Huang[a], Victor Fung[a], Zili Wu[b,c], De-en Jiang[a,*]

[a] Department of Chemistry, University of California, Riverside, CA 92521, United States
[b] Chemical Sciences Division, Oak Ridge National Laboratory, Oak Ridge, TN 37831, United States
[c] Center for Nanophase Materials Sciences, Oak Ridge National Laboratory, Oak Ridge, TN 37831, United States

ARTICLE INFO

Keywords:
Density functional theory
Reaction pathway
Surface chemistry
Indium oxide
Ethanol
Propene

ABSTRACT

It is highly desirable to convert bioethanol to value-added chemicals. As such, conversion of ethanol to propene (ETP) is attractive because propene is an important raw material for the production of plastics. In_2O_3 has shown promising catalytic performance for ETP conversion. However, the underlying mechanisms remain elusive. In this work, we use density functional theory (DFT) to investigate ETP reaction pathways on the In_2O_3 (110) surface. We find that the ETP reactions proceed through three major stages: ethanol to acetaldehyde, acetaldehyde to acetone, and acetone to propene. The ethanol-to-acetaldehyde step is kinetically facile. Comparing the two pathways from acetaldehyde to acetone, we show that the aldol reaction pathway via direct coupling of two acetaldehyde is more favorable than the acetate-ketonization pathway. The acetone-to-propene process is found to be the rate-limiting step of the overall reaction. This work provides a detailed mechanistic view of the ETP chemistry on In_2O_3(110) that paves the way for further exploration of effects such as surface termination, surface doping, and co-feeding of H_2 and H_2O on selectivity and catalyst stability.

1. Introduction

Bioethanol, produced through the process of fermentation of biomass such as corn, sugar canes or switchgrass, has been widely used as a drop-in fuel in the automobile industry [1–4]. More important, bioethanol can be converted to value-added chemicals such as acetone, isobutene, and propene [5–7]. Because propene is one of the most important feedstocks in chemical industry, catalytic conversion of ethanol to propene (ETP) has drawn some recent research interest [8,9].

In searching for ETP catalysts, initial attention focused on zeolites such as Ni-MCM41 and HZSM-5 because of their impressive catalytic performance in oligomerization and metathesis reactions of ethylene, after the dehydration of ethanol [10–13]. However, these catalysts suffered from low selectivity toward propene (only about 15%–30%) and poor stability [14–16]. Recent research has explored ways to improve their selectivity and stability [17].

Metal oxides such as CeO_2, ZrO_2, and In_2O_3 have also been tested for ETP [18–22]. For example, a yttria-ceria solid solution displayed stable catalytic performance and reasonably good propene selectivity (30%) [18,21]. Furthermore, some ZrO_2-based materials have shown propene yields of 40% [23]. Among the metal oxides, In_2O_3 is of particular interest because it gives the highest propene yield, though quickly deactivates over time [24–26]. With co-feeding of 8.5% H_2O and 30% H_2, Sc-doped In_2O_3 demonstrates 61% propene selectivity and high stability [26]. Moreover, a recent study reported that In_2O_3 composite materials (In_2O_3 and β-zeolite) also exhibit improved propene selectivity because the β-zeolite enhances the acetone to propene conversion [27].

Although these In_2O_3-based materials show promising catalytic performance for ETP reactions, the underlying ETP reaction mechanisms on In_2O_3 are still not well understood. To this end, this work aims to provide a fundamental understanding of ETP reactions on the In_2O_3 surface, by employing density functional theory to investigate the elementary reaction pathways. Our goal is to lay a foundation for further exploration of the ETP reactions on metal oxides and their advanced forms (such as doped ones and composite materials).

2. Methodology

The Vienna Ab Initio Simulation Package (VASP) was used to perform all calculations with periodic boundary conditions [28]. The Perdew-Burke-Ernzerhof (PBE) functional was employed to describe electron exchange and correlation [29]. The Projector Augmented Wave (PAW) method was used to describe the interaction between the

* Corresponding author.
E-mail address: djiang@ucr.edu (D.-e. Jiang).

https://doi.org/10.1016/j.cattod.2019.05.035
Received 1 February 2019; Received in revised form 7 May 2019; Accepted 16 May 2019
Available online 17 May 2019
0920-5861/

core and the valence electrons [30,31]. A kinetic energy cutoff of 450 eV was used for the planewave basis set. Structure relaxation was achieved by optimizing all ionic positions until the force was less than 0.01 eV/Å. Climbing-Image Nudged-Elastic-Band (CI-NEB) calculations were performed to search the minimum-energy pathways, with a force criterion of 0.05 eV/Å [32,33].

The In_2O_3 (110) surface was cleaved from the $(1\times\sqrt{2})$ supercell of the In_2O_3 bixbyite bulk structure. The In_2O_3 bulk unit cell was optimized and displayed a cell parameter of 10.31 Å, which shows a reasonable good agreement with the experimental value [34]. The slab model consists of 32 In atoms and 48 O atoms. The In_2O_3(110) slab contains four atomic layers and the Brillouin zone was sampled using a $(3\times3\times1)$ Monkhorst–Pack k-mesh. The bottom two layers were fixed to their equilibrium bulk position, while the top two layers and adsorbates were allowed to relax. A vacuum layer of 15 Å was added in z direction to avoid interactions between slabs. The adsorption energy was calculated as $E_{ad} = E_{slab+adsorbate} - E_{slab} - E_{adsorbate}$, where $E_{slab+adsorbate}$, E_{slab}, and $E_{adsorbate}$ denote the energy of the In_2O_3 slab with the adsorbate, the clean slab, and an isolated adsorbate, respectively.

3. Results and discussion

3.1. Structure of In_2O_3 and its (110) surface

The most stable In_2O_3 crystal has a body-centered-cubic bixbyite structure and the unit cell is in the space group symmetry of $Ia\bar{3}$. Each unit cell contains 32 indium atoms and 48 oxygen atoms (Fig. 1a). For In_2O_3, the (110) and (111) surfaces are the most stable [35]. The In_2O_3 (110) surface is stoichiometric and its termination has a relatively simple atomic surface structure when compared to the (111) surface. As a good starting point for a computational work, we focus on the (110) surface in this work and will address the (111) surface in the future.

Fig. 1a also shows the (110) cleavage plane through the bulk structure, while Fig. 1b and c show the top and side views of the In_2O_3 (110) slab, respectively. The top layer of the In_2O_3 (110) surface consists of chain-like repeating units, with each chain composed of two four-member In-O rings and one In-O-In chain (Fig. 1b). The surface structure contains four different types of In atoms: In1 and In4 are four-coordinated, while In2 and In3 are five-coordinated (Fig. 1b). Since both four-coordinated and five-coordinated In atoms are cleaved from the six-coordinated In atoms from the bulk structure, all In atoms on the surface are coordinatively unsaturated (*cus*). These *cus* In atoms can serve as surface sites for adsorbates and intermediates.

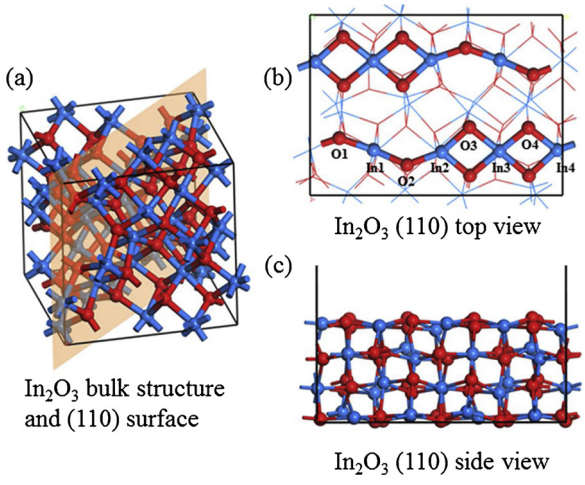

Fig. 1. (a) The In_2O_3 bulk structure and the (110) surface slice. (b) Top view of the In_2O_3 (110) slab model; top surface layer in ball-and-stick model, bottom three layers in line model. (c) Side view of the In_2O_3 (110) slab model. In, blue; O, red (For interpretation of the references to colour in this figure legend, the reader is referred to the web version of this article.).

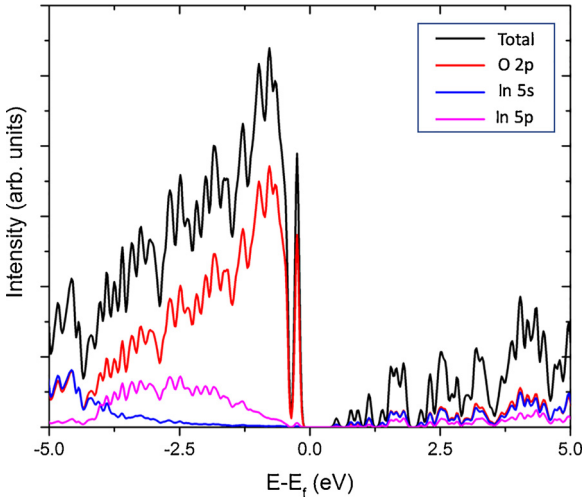

Fig. 2. Total and projected density of states of the In_2O_3(110) surface.

The total and projected density of states for In_2O_3 (110) are shown in Fig. 2. One can see that a small band gap is maintained for the In_2O_3 (110) surface. The valence-band maximum is dominated by the O 2p states, while the first few peaks in the conduction-band minimum are mainly originated from the In 5s5p states. These electronic states are important in adsorption and reaction of ethanol molecules on the surfaces, as explored next.

3.2. Ethanol adsorption on In_2O_3(110)

Due to its partially negative charge, the −OH group of ethanol prefers to interact with a metal center on an oxide surface. Table 1 summarizes the ethanol adsorption energies at various In atoms on In_2O_3 (110). In1 has the strongest adsorption among all the In atoms. One can also see the correlation between the coordination number and the adsorption energy: the four-coordinated In atoms (In1 and In4) exhibit stronger adsorption (more negative adsorption energies) than the five-coordinated In atoms (In2 and In3).

Fig. 3 shows the structure of the most stable site for ethanol adsorption on In_2O_3 (110) surface at the In1 site. The oxygen atom from ethanol adsorbs on top of the In atom, with an In-O distance of 2.28 Å, while the hydrogen atom from the ethanol hydroxyl group closely interacts with an In_2O_3 surface oxygen with an H−O distance of 1.85 Å. There are some short contacts between H atoms on the ethyl group and the surface O atoms (Fig. 3 left). The total Bader charge on the adsorbed ethanol molecule is +0.10 |e|, suggesting a partial electron transfer from the ethanol to the surface.

To understand why the four-coordinate In site is more active than the five-coordinate In site, we have analyzed the local density of states on In1 (C.N. = 4) and In2 (C.N. = 5) of the In_2O_3(110) surface. As shown in Fig. 4, a big difference between the two is In1's large peak around 1.5 eV (mainly 5s states with minor contribution from 5p

Table 1
Ethanol adsorption energy (E_{ad}) on different In atom sites (Fig. 1b) of In_2O_3(110). The coordination numbers of the In atoms by lattice O (C.N.) are also given.

Site	C.N.	E_{ad} (eV)
In1	4	−1.00
In2	5	−0.61
In3	5	−0.64
In4	4	−0.86

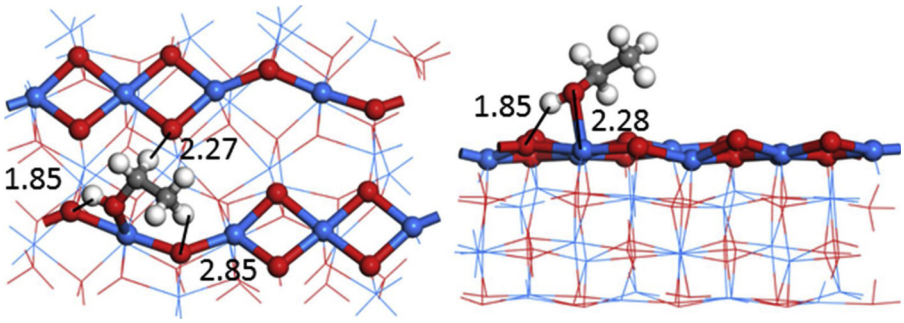

Fig. 3. Top view (left) and side view (right) of ethanol adsorption structure at the In1 site on In_2O_3(110). The key distances are labelled in Å. In, blue; O, red; C, grey; H, white (For interpretation of the references to colour in this figure legend, the reader is referred to the web version of this article.).

states), just above the Fermi level. This empty state, as a result of less coordination from O atoms of the oxide, plays a key role in adsorbing ethanol more strongly, as it interacts greatly with the O states of ethanol. Table 1 also shows that there is a slight difference between In1 and In2 in their reactivity, though both are four-coordinate. This indicates that the local geometry of the first-coordination shell of O atoms around an In atom is also important. In1 has two of the four oxygens exposed on the surface, while In4 has three of the four exposed, so In1 is less sterically hindered in adsorbing ethanol. Our subsequent computational modeling of the ETP chemistry is hence based on this configuration where ethanol molecules are adsorbed on the In1 sites.

3.3. Main pathways of ethanol to propene (ETP) conversion

Although there is a lack of detailed studies of ETP reaction pathways on the In_2O_3 surface, previous experimental studies [8,18,25] have concluded that acetaldehyde and acetone are two important intermediates of ETP reactions. Based on these two important intermediates, we propose that the whole ETP reactions can be divided into three stages (Scheme 1). In stage 1, ethanol dehydrogenates to acetaldehyde. In stage 2, acetaldehyde converts to acetone through two likely reaction pathways: in pathway 1, acetaldehyde undergoes a direct-coupling reaction and then a decarboxylation reaction to produce acetone; in pathway 2, acetaldehyde first converts to surface acetates which then undergoes a ketonization reaction to produce acetone. In stage 3, acetone is converted to propene. In order to identify the detailed mechanism for each pathway, we used DFT to investigate the elementary steps along the main pathways in Scheme 1.

3.4. Ethanol to acetaldehyde

Experimental studies [8,18,25] suggested that acetaldehyde is the very first intermediate in the ETP reaction. So we hypothesize that the ETP reaction starts with ethanol dehydrogenation to acetaldehyde. To test this idea, we first investigated the ethanol to acetaldehyde conversion on the In_2O_3 (110) surface. Fig. 5 shows the reaction pathway and the structures along the path. The ethanol to acetaldehyde conversion is exothermic and involves two dehydrogenation steps. The first step is the dehydrogenation of the hydroxyl group of ethanol. This elementary step is very facile and has a very low activation energy (0.13 eV). The second step is the dehydrogenation of the α carbon on the ethoxy group to form acetaldehyde. This elementary step requires an activation energy of 0.81 eV. Since both dehydrogenation steps require rather low activation energies, the ethanol-to-acetaldehyde conversion on In_2O_3(110) is predicted to be facile.

3.5. Direct coupling of acetaldehyde to form acetone

In the next stage (Stage 2), acetaldehyde can couple to form acetone on the In_2O_3 (110) surface via Pathway 1 (Scheme 1). Fig. 6 shows the elementary steps of the coupling process. First, two acetaldehyde molecules are adsorbed at two neighboring In sites (In1and In2) initially (i). Then, the acetaldehyde adsorbed on the In2 site undergoes cleavage of a C—H bond on the methyl group and tautomerizes to the enolate form (ii). This is followed by C—C coupling between acetaldehyde and enolate where the β-C of enolate attacks the aldehyde group of acetaldehyde at the In1 site (TS2), as in an aldol reaction. In the same step, the α-C of enolate further dehydrogenates and forms a new bond with a surface lattice oxygen, forming a carboxylate group. The newly formed intermediate, β-oxidobutyrate (iii), shows a significantly lower energy than the species in the previous step. Next, the β-oxidobutyrate intermediate undergoes β-H elimination (TS3) to form acetoacetate (iv). Then, the acetoacetate intermediate undergoes a decarboxylation reaction (TS4), to form acetone enolate (v). This elementary step is endothermic by 1.0 eV and generates an oxygen vacancy on the surface. After CO_2 desorption, the acetone enolate intermediate (vi) extracts a hydrogen atom from a surface hydroxyl group (TS5), forming an acetone molecule on the In_2O_3 surface (vii). Both the coupling step (ii → iii) and the dehydrogenation of β-oxidobutyrate step (iii → iv) require relatively high activation energies (1.46 eV and 1.48 eV), which are likely the rate-limiting steps for acetaldehyde to acetone conversion.

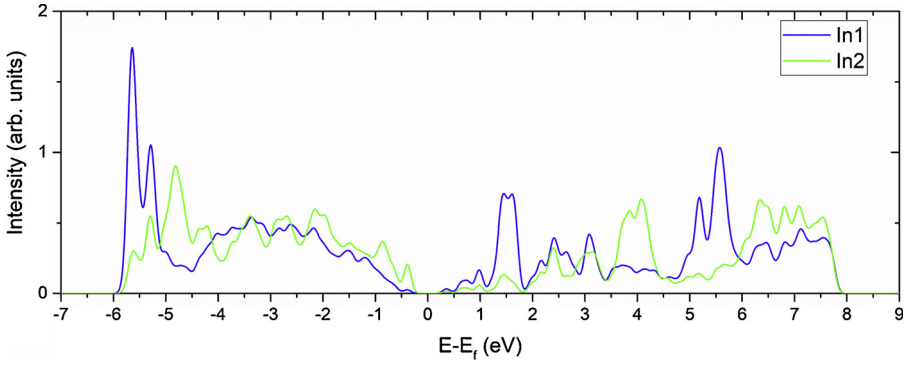

Fig. 4. Site-projected local density of states In1 and In2 sites of the pristine In_2O_3(110) surface (Fig. 1b).

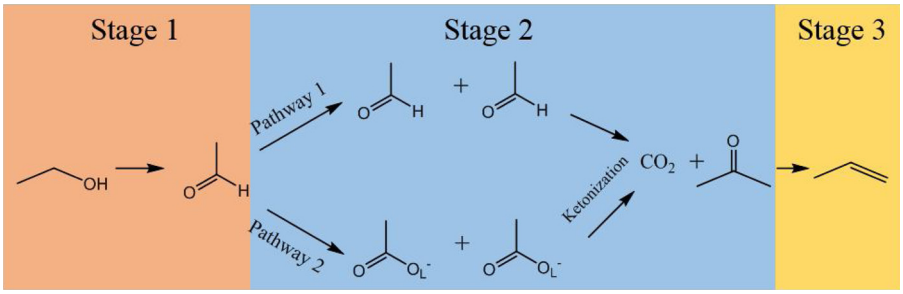

Scheme 1. Proposed reaction scheme of ethanol to propene (ETP) conversion on $In_2O_3(110)$. O_L indicates a lattice oxygen atom.

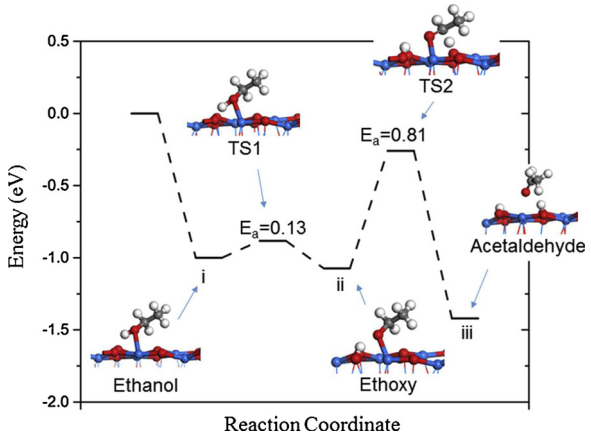

Fig. 5. Reaction pathway from ethanol to acetaldehyde on $In_2O_3(110)$.

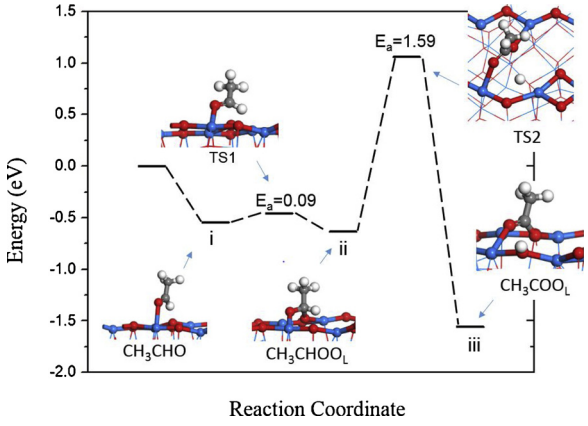

Fig. 7. Reaction pathway from acetaldehyde to acetate on In_2O_3 (110).

3.6. Acetaldehyde to acetate and ketonization of acetate to form acetone

In Stage 2 of Scheme 1, the acetone formation can also proceed via an alternative pathway through ketonization of acetate species on the In_2O_3 surface (Pathway 2). So we also investigated this mechanism. We first examined the acetaldehyde-to-acetate reaction on $In_2O_3(110)$. As shown in Fig. 7, the aldehyde group of the adsorbed acetaldehyde molecule (i) first reacts with a lattice oxygen atom via a very small barrier (TS1), forming a CH_3CHOO_L intermediate (ii; O_L denotes a lattice oxygen). Then, CH_3CHOO_L further dehydrogenates to form a surface acetate group and a surface hydroxyl (iii). This elementary step requires an activation energy of 1.59 eV.

The surface acetates from acetaldehyde can undergo a ketonization reaction to produce acetone and CO_2, as shown in Fig. 8. The reaction starts with two surface acetates adsorbed next to each other (i). Then one methyl group of a surface acetate loses a hydrogen atom (TS1), forming a CH_2COO_L intermediate (ii). Interesting to note, the

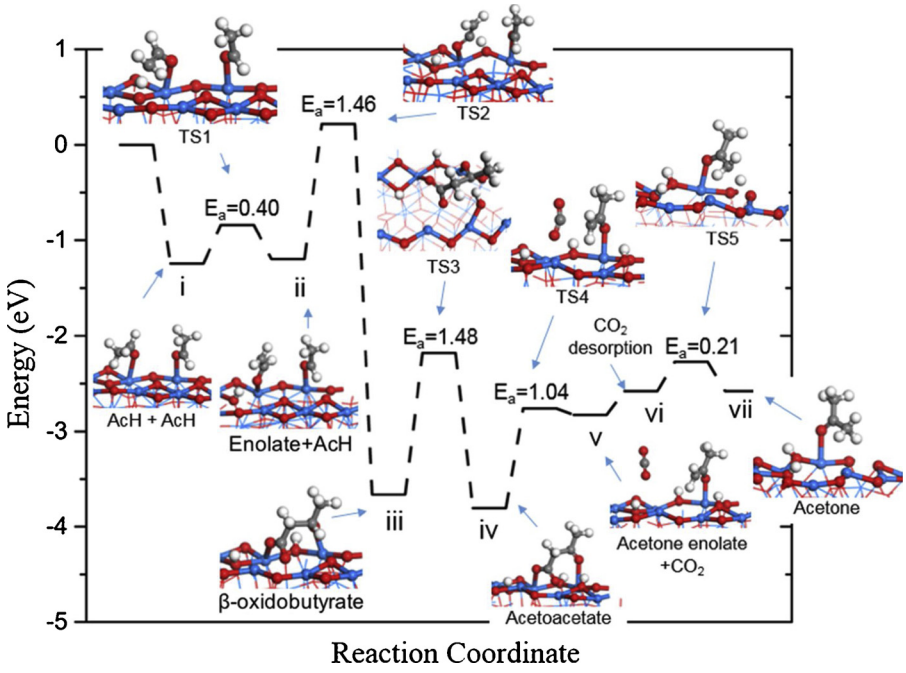

Fig. 6. Reaction pathway for direct coupling of two acetaldehyde molecules to form acetone on $In_2O_3(110)$. AcH, acetaldehyde.

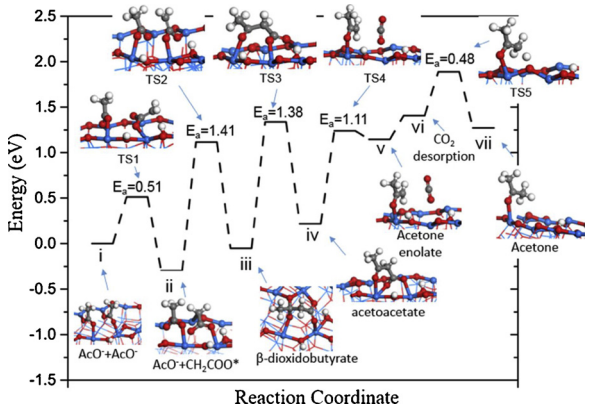

Fig. 8. Reaction pathway for ketonization of acetate to form acetone on In_2O_3 (110). Ac = CH_3CO.

unsaturated C_α atom of CH_2COO_L binds to an In atom on In_2O_3 surface. Next, the C_α of CH_2COO_L lifts from the surface and attacks the carboxylate carbon of the other surface acetate (TS2), forming a β-dioxidobutyrate intermediate (iii). This step is slightly endothermic and requires an activation energy of 1.41 eV. Then, the reaction is followed by breaking one of the C_β-oxido bond of β-dioxidobutyrate (TS3), forming an acetoacetate intermediate (iv). This elementary step has an activation energy of 1.38 eV. It should be noted that the acetoacetate intermediate is also observed in the acetaldehyde to acetone conversion in Pathway 1 (Fig. 6). So the remaining steps from acetoacetate to acetone are similar: acetoacetate undergoes decarboxylation first, creating an acetone enolate which then extracts a surface hydrogen to acetone.

3.7. From acetone to propene

In the last stage (Stage 3) of Scheme 1, acetone is converted to propene. Fig. 9 shows the minimum-energy pathway starting with an adsorbed acetone and a nearby hydroxyl group (i). The surface hydrogen atom can be obtained from the previous dehydrogenation process of ethanol or acetaldehyde. In the first step, one surface hydrogen reacts with the carbonyl group of the acetone molecule (TS1), forming an isopropoxy intermediate (ii). Although relatively difficult on oxide surfaces, hydrogenation reaction on In_2O_3 has been demonstrated recently [36–38]. Next, the C—O bond and one CH_2—H bond of the isopropoxy intermediate break (TS2), leading to propene formation (iii). The propene molecule weakly adsorbs on the In_2O_3 surface and can be easily desorbed. After breaking from isopropoxy, the oxygen atom returns to the lattice, replenishing the oxygen vacancy site that was created during the CO_2 formation in the previous steps. The overall

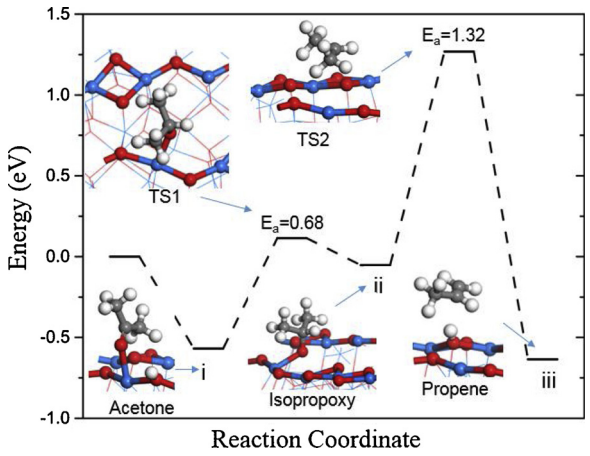

Fig. 9. Reaction pathway from acetone to propene on In_2O_3(110).

profile of the acetone-to-propene conversion (Fig. 9) suggests a barrier of 1.8 eV (from i to TS2).

After completing the DFT-energy profiles for the pathways as shown in Scheme 1, one arrives at a few points. First, the ethanol-to-acetaldehyde step is kinetically facile. Second, comparing the two pathways from acetaldehyde to acetone, one finds that the aldol reaction pathway via direct coupling of two acetaldehyde (Pathway 1 in Scheme 1) is more favorable than the acetate-ketonization pathway (Pathway 2 in Scheme 1). This is due to both the difficulty in acetate formation (Fig. 7) and the continuing uphill process in the acetate-to-acetone process (Fig. 8). Third, the acetone-to-propene process is more difficult (barrier: 1.8 eV) than the acetaldehyde-to-acetone process via Pathway 1 (barrier: 1.5 eV).

3.8. Implications

Recently, Iwamoto et al. investigated ETP reaction on In_2O_3 and conducted detailed mechanistic studies on Sc-doped In_2O_3. Based on pulse reaction experiments, they found acetaldehyde, acidic acid, and acetone to be key intermediates [24]. They further proposed that acetaldehyde was first converted to acidic acid by reacting with the surface hydroxyl group, and then the resulting acetic acid yielded acetone and carbon dioxide via the ketonization reaction [24]. Our DFT results suggest that the direct coupling of acetaldehyde is more likely. However, the difficulty in the acetone-to-propene process could also make the acetate-to-acetone channel open. Iwamoto et al. reported a relatively high amount of unreacted acetaldehyde and acetone in pulse experiment, suggesting that acetaldehyde coupling and acetone hydrogenation may be the rate-limiting steps. Our DFT calculation confirmed that acetone hydrogenation is indeed the rate-limiting step. This also helps in explaining the effect of co-feeding hydrogen in the ETP reaction: the co-fed H_2 can promote the hydrogenation of acetone, thus promoting the propene formation. But we note that the In_2O_3 catalyst may undergo phase change during prolonged catalysis to metallic In or In_2O_3 clusters, which is still challenging for DFT to model and might account for some differences between our results and the experimental literature.

4. Conclusions

We have studied the ethanol to propene (ETP) conversion on the In_2O_3 (110) pristine surface by density functional theory. Ethanol molecules were found to strongly chemisorb on In_2O_3 (110) surface. Among In atom adsorption sites, the In1 sites show the highest adsorption energy due to their low coordination number (four). The ethanol to acetaldehyde conversion was found to be facile on the In_2O_3 surface, with an activation energy of 0.87 eV. The acetaldehyde to acetone conversion was investigated through two possible reaction pathways. In the first reaction pathway, acetaldehyde dehydrogenates and then couples to another acetaldehyde via the aldol reaction, then leading to a β-oxidobutyrate intermediate before acetone formation. In the second reaction pathway, the acetaldehyde molecules are first oxidized to surface acetates, then undergoing ketonization to produce the acetone product. We found that the directing coupling of acetaldehyde is more likely, leading to acetone. The acetone to propene conversion was found to go through isopropoxy intermediates and to be the rate-limiting step of the overall reaction. This work provides an in-depth understanding of ETP reaction on In_2O_3 (110) and we hope to further explore the role of dopants such as Sc in controlling the selectivity in future.

Acknowledgements

This research is sponsored by the U.S. Department of Energy, Office of Science, Office of Basic Energy Sciences, Chemical Sciences, Geosciences, and Biosciences Division. This research used resources of

the National Energy Research Scientific Computing Center, a DOE Office of Science User Facility supported by the Office of Science of the U.S. Department of Energy under Contract No. DE-AC02-05CH11231.

References

[1] J. Baeyens, Q. Kang, L. Appels, R. Dewil, Y. Lv, T. Tan, Challenges and opportunities in improving the production of bio-ethanol, Prog. Energy Combust. Sci. 47 (2015) 60–88.

[2] H.B. Aditiya, T.M.I. Mahlia, W.T. Chong, H. Nur, A.H. Sebayang, Second generation bioethanol production: a critical review, Renew. Sustain. Energy Rev. 66 (2016) 631–653.

[3] H. Zabed, J.N. Sahu, A. Suely, A.N. Boyce, G. Faruq, Bioethanol production from renewable sources: current perspectives and technological progress, Renew. Sustain. Energy Rev. 71 (2017) 475–501.

[4] V. Zacharopoulou, A. Lemonidou, Olefins from biomass intermediates: a review, Catalysts 8 (2018) 2.

[5] J. Sun, Y. Wang, Recent advances in catalytic conversion of ethanol to chemicals, ACS Catal. 4 (2014) 1078–1090.

[6] J. Goldemberg, Ethanol for a sustainable energy future, Science 315 (2007) 808–810.

[7] G.W. Huber, S. Iborra, A. Corma, Synthesis of transportation fuels from biomass: chemistry, catalysts, and engineering, Chem. Rev. 106 (2006) 4044–4098.

[8] M. Iwamoto, Selective catalytic conversion of bio-ethanol to propene: a review of catalysts and reaction pathways, Catal. Today 242 (2015) 243–248.

[9] X. Li, A. Kant, Y. He, H.V. Thakkar, M.A. Atanga, F. Rezaei, D.K. Ludlow, A.A. Rownaghi, Light olefins from renewable resources: selective catalytic dehydration of bioethanol to propylene over zeolite and transition metal oxide catalysts, Catal. Today 276 (2016) 62–77.

[10] K. Ikeda, Y. Kawamura, T. Yamamoto, M. Iwamoto, Effectiveness of the template-ion exchange method for appearance of catalytic activity of Ni–MCM-41 for the ethene to propene reaction, Catal. Commun. 9 (2008) 106–110.

[11] M. Iwamoto, Y. Kosugi, Highly selective conversion of ethene to propene and butenes on nickel ion-loaded mesoporous silica catalysts, J. Phys. Chem. C 111 (2007) 13–15.

[12] W. Xia, A. Takahashi, I. Nakamura, H. Shimada, T. Fujitani, Study of active sites on the MFI zeolite catalysts for the transformation of ethanol into propylene, J. Mol. Catal. A Chem. 328 (2010) 114–118.

[13] J. Huangfu, D. Mao, X. Zhai, Q. Guo, Remarkably enhanced stability of HZSM-5 zeolite co-modified with alkaline and phosphorous for the selective conversion of bio-ethanol to propylene, Appl. Catal. A Gen. 520 (2016) 99–104.

[14] W. Xia, F. Wang, X. Mu, K. Chen, A. Takahashi, I. Nakamura, T. Fujitani, Catalytic performance of H-ZSM-5 zeolites for conversion of ethanol or ethylene to propylene: effect of reaction pressure and SiO_2/Al_2O_3 ratio, Catal. Commun. 91 (2017) 62–66.

[15] Z. Song, A. Takahashi, N. Mimura, T. Fujitani, Production of propylene from ethanol over ZSM-5 zeolites, Catal. Lett. 131 (2009) 364–369.

[16] K. Inoue, K. Okabe, M. Inaba, I. Takahara, K. Murata, Catalytic conversion of ethanol to propylene by H-ZSM-11, React. Kinet. Catal. Lett. 101 (2010) 227–235.

[17] N. Zhang, D. Mao, X. Zhai, Selective conversion of bio-ethanol to propene over nano-HZSM-5 zeolite: remarkably enhanced catalytic performance by fluorine modification, Fuel Process. Technol. 167 (2017) 50–60.

[18] F. Hayashi, M. Iwamoto, Yttrium-modified ceria as a highly durable catalyst for the selective conversion of ethanol to propene and ethene, ACS Catal. 3 (2013) 14–17.

[19] W. Xia, F. Wang, X. Mu, K. Chen, A. Takahashi, I. Nakamura, T. Fujitani, Highly selective catalytic conversion of ethanol to propylene over yttrium-modified zirconia catalyst, Catal. Commun. 90 (2017) 10–13.

[20] F. Wang, W. Xia, X. Mu, K. Chen, H. Si, Z. Li, A combined experimental and theoretical study on ethanol conversion to propylene over Y/ZrO_2 catalyst, Appl. Surf. Sci. 439 (2018) 405–412.

[21] F. Hayashi, M. Tanaka, D. Lin, M. Iwamoto, Surface structure of yttrium-modified ceria catalysts and reaction pathways from ethanol to propene, J. Catal. 316 (2014) 112–120.

[22] Ld.R. Silva-Calpa, P.C. Zonetti, D.C. de Oliveira, R.R. de Avillez, L.G. Appel, Acetone from ethanol employing $ZnxZr_1-xO_2-y$, Catal. Today 289 (2017) 264–272.

[23] W. Xia, F. Wang, X. Mu, K. Chen, Transformation of ethanol to propylene on ZrO_2 catalysts: effect of reaction conditions on the catalytic performance, React. Kinet. Catal. Lett. 122 (2017) 463–472.

[24] M. Iwamoto, M. Tanaka, S. Hirakawa, S. Mizuno, M. Kurosawa, Pulse and IR study on the reaction pathways for the conversion of ethanol to propene over scandium-loaded indium oxide catalysts, ACS Catal. 4 (2014) 3463–3469.

[25] M. Iwamoto, S. Mizuno, M. Tanaka, Direct and selective production of propene from bio-ethanol on Sc-loaded In_2O_3 catalysts, Chem. Eur. J. 19 (2013) 7214–7220.

[26] S. Mizuno, M. Kurosawa, M. Tanaka, M. Iwamoto, One-path and selective conversion of ethanol to propene on scandium-modified indium oxide catalysts, Chem. Lett. 41 (2012) 892–894.

[27] F. Xue, C. Miao, Y. Yue, W. Hua, Z. Gao, Direct conversion of bio-ethanol to propylene in high yield over the composite of In_2O_3 and zeolite beta, Green. Chem. 19 (2017) 5582–5590.

[28] G. Kresse, J. Furthmüller, Efficient iterative schemes for ab initio total-energy calculations using a plane-wave basis set, Phys. Rev. B 54 (1996) 11169–11186.

[29] J.P. Perdew, K. Burke, M. Ernzerhof, Generalized gradient approximation made simple, Phys. Rev. Lett. 77 (1996) 3865–3868.

[30] P.E. Blöchl, Projector augmented-wave method, Phys. Rev. B 50 (1994) 17953–17979.

[31] G. Kresse, D. Joubert, From ultrasoft pseudopotentials to the projector augmented-wave method, Phys. Rev. B 59 (1999) 1758–1775.

[32] G. Henkelman, H. Jónsson, Improved tangent estimate in the nudged elastic band method for finding minimum energy paths and saddle points, J. Chem. Phys. 113 (2000) 9978–9985.

[33] G. Henkelman, B.P. Uberuaga, H. Jónsson, A climbing image nudged elastic band method for finding saddle points and minimum energy paths, J. Chem. Phys. 113 (2000) 9901–9904.

[34] M. Marezio, Refinement of the crystal structure of In_2O_3 at two wavelengths, Acta Crystallogr. 20 (1966) 723–728.

[35] A. Walsh, C.R.A. Catlow, Structure, stability and work functions of the low index surfaces of pure indium oxide and Sn-doped indium oxide (ITO) from density functional theory, J. Mater. Chem. 20 (2010) 10438–10444.

[36] D. Albani, M. Capdevila-Cortada, G. Vilé, S. Mitchell, O. Martin, N. López, J. Pérez-Ramírez, Semihydrogenation of acetylene on indium oxide: proposed single-ensemble catalysis, Angew. Chem. Int. Ed. 56 (2017) 10755–10760.

[37] J. Ye, C. Liu, D. Mei, Q. Ge, Active oxygen vacancy site for methanol synthesis from CO_2 hydrogenation on In_2O_3(110): a DFT study, ACS Catal. 3 (2013) 1296–1306.

[38] M. Dou, M. Zhang, Y. Chen, Y. Yu, DFT study of In_2O_3-catalyzed methanol synthesis from CO_2 and CO hydrogenation on the defective site, New J. Chem. 42 (2018) 3293–3300.